In vivo Optical Molecular Imaging of Vascular Endothelial Growth Factor for Monitoring Cancer Treatment

Sung K. Chang, Imran Rizvi, Nicolas Solban, and Tayyaba Hasan

Abstract

Purpose: Vascular endothelial growth factor (VEGF) expression is a critical component in tumor growth and metastasis. Capabilities to monitor VEGF expression *in vivo* can potentially serve as a useful tool for diagnosis, prognosis, treatment planning, monitoring, and research. Here, we present the first report of *in vivo* hyperspectral molecular imaging strategy capable of monitoring treatment-induced changes in VEGF expression.

Experimental Design: VEGF was targeted with an anti-VEGF antibody conjugated with a fluorescent dye and was imaged *in vivo* using a hyperspectral imaging system. The strategy was validated by quantitatively monitoring VEGF levels in three different tumors as well as following photodynamic treatment. Specificity of the molecular imaging strategy was tested using *in vivo* competition experiments and mathematically using a quantitative pharmacokinetic model.

Results: The molecular imaging strategy successfully imaged VEGF levels quantitatively in three different tumors and showed concordance with results from standard ELISA. Changes in tumoral VEGF concentration following photodynamic treatment and Avastin treatment were shown. Immunohistochemistry shows that (*a*) the VEGF-specific contrast agent labels both proteoglycan-bound and unbound VEGF in the extracellular space and (*b*) the bound VEGF is released from the extracellular matrix in response to photodynamic therapy. *In vivo* competition experiments and quantitative pharmacokinetic model-based analysis confirmed the high specificity of the imaging strategy.

Conclusion: This first report of *in vivo* quantitative optical molecular imaging-based monitoring of a secreted cytokine in tumors may have implications in providing tools for mechanistic investigations as well as for improved treatment design and merits further investigation.

The critical role vascular endothelial growth factor (VEGF) plays in angiogenesis as well as the development of primary, recurrent, and metastatic disease has made it the focus of several investigations as a clinical biomarker for diagnosis, prognosis, and treatment monitoring (1). The role of VEGF in the overall tumor development and treatment response is complex and may depend on the site, individual subjects, and the type of the malignancy (2–6). In particular, several studies (7–9) showed that cancer treatments including photodynamic therapy (PDT), radiotherapy, and chemotherapy can lead to increased tumoral VEGF expression and subsequently to more aggressive disease (10, 11). It would therefore be very useful to establish VEGF levels *in vivo* and *in situ* to clearly understand the significance of its expression and alterations both from a mechanistic viewpoint and for the design of improved combination protocols. However, current biochemical assays that determine VEGF concentration *ex vivo* or from circulation are either invasive and/or limited in sensitivity. Circulating VEGF has been evaluated as a surrogate marker for tumor angiogenesis as well as prognosis only with mixed success, as it is not only specific to tumoral VEGF but also reflects those secreted by other cells such as platelets, granulocytes, monocytes, mast cells, and lymphocytes (12). VEGF levels have also been evaluated directly from the tumor using *ex vivo* techniques such as immunohistochemistry, but they are invasive, semiquantitative, capture only a temporal snapshot and suffer from procedural variability (4, 13, 14).

Molecular imaging has enabled direct visualization of various molecular targets such as statically anchored cell-surface proteins (15) and enzymatic proteins (16). Similar strategy can lead to *in vivo*, *in situ*, quantitative monitoring of not only the overall VEGF expression but also its temporal dynamics and spatial distribution. Capabilities to monitor the spatio-temporal dynamics of VEGF may provide important insights for diagnosis, prognosis, and therapeutic design (17–19). However, *in vivo* molecular imaging of dynamically secreted cytokines such as VEGF is not developed. A previous study (20) investigated the biodistribution of a radiolabeled anti-VEGF antibody in tumors but did not address the capabilities

Authors' Affiliation: Wellman Center for Photomedicine, Massachusetts General Hospital, Harvard Medical School, Boston, Massachusetts

Received 10/3/07; revised 3/16/08; accepted 3/21/08.

Grant support: NIH grant P01 CA84203.

The costs of publication of this article were defrayed in part by the payment of page charges. This article must therefore be hereby marked *advertisement* in accordance with 18 U.S.C. Section 1734 solely to indicate this fact.

Note: Supplementary data for this article are available at Clinical Cancer Research Online (http://clincancerres.aacrjournals.org/).

Current address for I. Rizvi: Thayer School of Engineering, Dartmouth College, Hanover, NH. Current address for N. Solban: Acceleron Pharma, 24 Emily Street, Cambridge, MA 02139.

Requests for reprints: Tayyaba Hasan, Wellman Center for Photomedicine, Massachusetts General Hospital, Harvard Medical School, 40 Blossom Street, Boston MA 02114. Phone: 617-726-6996; Fax: 617-726-8566; E-mail: thasan@partners.org.

doi:10.1158/1078-0432.CCR-07-4536

or limitations of *in vivo* VEGF monitoring. In the present study, we report the development of an optical molecular imaging strategy to monitor tumoral VEGF expression *in vivo*. To our knowledge, this is the first systematic study to evaluate the capabilities and limitations of imaging VEGF expression using an exogenous contrast agent. We show that the molecular imaging strategy allows quantitative monitoring of tumoral VEGF levels in different tumor types as well as dynamic changes in VEGF expression following PDT and antiangiogenic therapy with high specificity. This method offers a quantitative and specific paradigm for monitoring the spatial and temporal dynamics of VEGF expression that can help mechanistic investigation of response to cancer therapy.

Materials and Methods

Materials. Avastin anti-VEGF antibody, MLN591 anti-prostate-specific membrane antigen antibody, C225 anti–epidermal growth factor receptor (EGFR) antibody, and benzoporphyrin derivative were a kind gift from Genentech, Millennium Pharmaceuticals, ImClone Systems, and QLT, respectively. Anti-PECAM-1 FITC-conjugated monoclonal antibody (CBL1337F), anti-perlecan antibody (ab23418), and Alexa Fluor 680 fluorescent dye were purchased from Chemicon, Abcam, and Invitrogen, respectively.

Conjugation of antibody with fluorescent dye. VEGF-specific contrast agent (CA_{VEGF}) was formulated by conjugating Avastin with Alexa Fluor 680 fluorescent dye with succinimidyl esters according to manufacturer's specifications. Briefly, 10 mg/mL Avastin (250 μL) was mixed with 1 mol/L sodium bicarbonate buffer (25 μL) and 10 mg/mL fluorescent dye (25 μL). The mixture was incubated for 1 h at room temperature. To separate the CA_{VEGF} from the unconjugated dye, the mixture was eluted in a PD-10 desalting column (Amersham Biosciences). MLN591 was conjugated with Alexa Fluor 680 fluorescent dye with succinimidyl ester in a similar manner. The antibody/fluorescent dye molar ratio resulting from the reaction was determined according to the manufacturer's specifications using the absorbance at 280 and 679 nm for the antibody and the fluorescent dye, respectively. All absorbance readings were measured in a quartz cuvette using the 8453 UV-visible spectrophotometer (Agilent Technologies). The average ± SE molar ratio from nine conjugations throughout the experiment was 5.96 ± 0.22, showing a high level of uniformity of the conjugation reaction.

Animals. PC-3 prostate cancer cells, AsPC-1 pancreatic cancer cells, or Capan-1 pancreatic cancer cells (3×10^6) in 50 μL Matrigel (BD Biosciences) were injected s.c. in both left and right hind flanks of severe combined immunodeficient mice. The tumor was allowed to grow to a size of 5 to 6 mm in 2 weeks. All animal studies were approved by the Subcommittee on Research Animal Care at the Massachusetts General Hospital.

In vivo *fluorescence imaging and calibration.* Either CA_{VEGF} or the MLN591-Alexa Fluor 680 conjugate (100 μg) was delivered via i.v. injection in the tail vein of the tumored mouse. A single injection of 100 μg Avastin in mice is a subtherapeutic dose that has not been shown to induce therapeutic effect on these tumors (data not shown). One hour following the delivery of the conjugated antibody, photosensitizer or PBS (100 μL) was injected i.v. in the tail vein in the PDT-treated mice and nontreated mice, respectively. PDT was then done according to the procedure outlined below. To allow sufficient tumoral delivery and target binding of the conjugated antibody, wavelength-resolved fluorescence hyperspectral images of the tumor were acquired with the Maestro imaging system (CRI) 24 h following the delivery of the conjugated antibody unless specified otherwise. The tumor was exposed during the imaging procedure to eliminate any potential optical distortion through skin and thus enhance accuracy of the model-based quantitative image analysis. A 615- to 665-nm excitation filter and a 700-nm long-pass emission filter (M-MSI-FLTR-640) were used to acquire fluorescence images of Alexa Fluor 680. Hyperspectral images were acquired between 700 and 800 nm at 10-nm intervals. Any potential variation in imaging system sensitivity was accounted for by calibrating spectrally unmixed CA_{VEGF} images with Oxazine 725 (Exciton), a highly photostable laser dye with fluorescence characteristics similar to Alexa Fluor 680 (21). A quartz cuvette containing 200 nmol/L Oxazine laser dye was imaged with the Maestro imaging system before each imaging session and subsequently acquired images were normalized by the fluorescence intensity of the laser dye. CA_{VEGF} fluorescence was quantified by spectrally unmixing Alexa Fluor 680 fluorescence spectrum with the tissue autofluorescence spectrum using linear least-squares optimization.

Photodynamic therapy. Photosensitizer was delivered to the tumored mouse by i.v. injection of 0.25 mg/kg benzoporphyrin derivative in the tail vein. One hour following photosensitizer delivery, an incision was made on the skin to expose the s.c. tumor and a 690-nm diode laser module (High Power Devices) was irradiated on the tumor at an irradiance of 100 mW/cm^2 and a fluence of 50 J/cm^2. Following PDT, the incision was closed using 9-mm wound clips (BD Diagnostics).

ELISA. Tumors were harvested 24 h following PDT and frozen in liquid nitrogen. The frozen tumors were pulverized with a tissue homogenizer and lysed in lysis buffer. The total protein concentration was determined using a standard Lowry method. A human VEGF DuoSet ELISA Development System (R&D Systems) was used to quantify human VEGF levels. Resulting VEGF concentrations were normalized by total protein concentration.

Immunofluorescence. To count the microvessel density (MVD), tumors were harvested immediately following *in vivo* fluorescence imaging. The tumors were embedded in OCT compound and sectioned into 5-μm-thick cryosections. The sections were air dried, fixed in acetone, and incubated with anti-mouse PECAM-1 FITC-conjugated antibody overnight at 4°C. Average MVD was calculated by averaging the number of CD31$^+$ vessel structures counted from five randomized fields per tumor section at a magnification of ×200 under the Olympus BX-51 fluorescence microscope.

To study tumoral localization of CA_{VEGF}, tumors were harvested 24 h following i.v. injection of CA_{VEGF} and PDT, embedded in OCT compound, and sectioned into 5-μm-thick cryosections. To stain for EGFR, the sections were blocked with 1% bovine serum albumin and incubated with C225 antibody-Alexa Fluor 488 conjugate overnight at 4°C. To stain for perlecan, the sections were fixed in acetone, blocked with 1% bovine serum albumin, and incubated with anti-perlecan antibody (ab23418)-Alexa Fluor 488 conjugate overnight at 4°C. Slides were imaged using a Leica LCS laser scanning confocal microscope with a ×100 oil immersion objective.

Model-based quantitative analysis. A standard curve to convert fluorescence intensity from the acquired images into CA_{VEGF} concentration was generated from fluorescence images of pulverized s.c. tumor mixed with known concentration (0, 5, 10, 20, and 30 nmol/L) of CA_{VEGF} loaded into 384-well plates. A mathematical pharmacokinetic model describing antibody uptake in solid tumors (22) was applied to estimate VEGF-bound and unbound tumoral CA_{VEGF} concentrations ($[CA_{VEGF}]_{Bound}$ and $[CA_{VEGF}]_{Free}$, respectively) from the contrast agent labeling. The model describes the temporal kinetics of $[CA_{VEGF}]_{Total}$ (sum of $[CA_{VEGF}]_{Bound}$ and $[CA_{VEGF}]_{Free}$) in the tumor compartment and $[CA_{VEGF}]_{Plasma}$ in the plasma compartment in terms of CA_{VEGF} binding affinity (K_a) and plasma pharmacokinetics (λ_1, λ_2), tumoral VEGF concentration (B_0), the vascular permeability-surface area product (PS), as well as the rate of antibody loss from the tumor (L).

Plasma compartment:

$$\frac{[CA_{VEGF}]_{Plasma}}{[CA_{VEGF}]_{Plasma,0}} = R\, e^{-\gamma_1 t} + (1-R)\, e^{-\gamma_2 t} \qquad (A)$$

Tumor compartment:

$$[CA_{VEGF}]_{Bound} = \frac{K_a\, B_0\, [CA_{VEGF}]_{Free}}{1 + K_a\, [CA_{VEGF}]_{Free}} \qquad (B)$$

$$[CA_{VEGF}]_{Total} = [CA_{VEGF}]_{Bound} + [CA_{VEGF}]_{Free} \quad (C)$$

$$\Phi \frac{d[CA_{VEGF}]_{Total}}{dt} = PS\,[CA_{VEGF}]_{Free} \quad (D)$$

Among the input variables to the model, the K_a of CA_{VEGF} was set to that of Avastin (9.1×10^8 mol/L^{-1}; ref. 23), as the molar ratio of antibody/fluorescent dye below 10 does not significantly affect the K_a (24–26). Initial and terminal circulation half-lives of CA_{VEGF}, λ_1 and λ_2, were set to those of Avastin (1.2 h and 6.81 days, respectively) measured in mice (27). Although not reported, the SD of the Avastin circulation half-life in mice is expected to be ±15% based on measurements in rats (27). B_0 was set to the results of the ELISA. The two unknown input variables (PS and L) were iteratively adjusted using the Gauss-Newton algorithm to fit the mathematical model to the observed contrast agent labeling. $[CA_{VEGF}]_{Bound}$ and $[CA_{VEGF}]_{Free}$ were then calculated using the estimated PS and L as well as the tumoral VEGF concentration, binding affinity, and murine circulation half-life of Avastin.

Statistics. Data are presented as mean ± SE. The significance of the difference between groups was evaluated with unpaired Student's t test. Pearson correlation coefficient (r) and the corresponding P value were used to investigate the strength and the significance of the correlation between CA_{VEGF} fluorescence and MVD, respectively. $P < 0.05$ was considered statistically significant.

Results

Monitoring VEGF levels in different tumors. We initially tested the molecular imaging strategy in s.c. tumors from three different human cancer cell lines that express different levels of VEGF: one from prostate cancer (PC-3) and two from pancreatic cancer (AsPC-1 and Capan-1). Temporal kinetics of CA_{VEGF} labeling in each tumor was monitored by acquiring images at 1, 3, 6, and 24 hours following i.v. injection of the CA_{VEGF}. The fluorescence intensity increased during the first 6 hours and leveled by 24 hours, suggesting that CA_{VEGF} uptake has saturated (Fig. 1A). To confirm that the fluorescent dye remains conjugated to the antibody throughout the 24-hour imaging period, we monitored the fluorescence of the unconjugated dye within the tumor following i.v. injection of an equivalent dose (4 nmol unconjugated Alexa Fluor 680). Ninety percent of the dye fluorescence cleared within 5 hours of injection (data not shown). The rapid clearance of the unconjugated dye suggests that the CA_{VEGF} fluorescence observed at 24 hours following injection originates from the fluorescent dye conjugated to Avastin. To validate that CA_{VEGF} labeling corresponds to tumoral VEGF levels, tumoral VEGF concentration was quantified *ex vivo* using ELISA. Good correlation with the results of the biochemical assay (Fig. 1B) shows that average fluorescence intensity of CA_{VEGF} labeling at 24 hours is indicative of VEGF levels in different tumor types.

In all three tumors, Pearson's statistic showed a linear association ($r = 0.64$, $P < 0.05$) between CA_{VEGF} fluorescence and MVD among the tumor samples from three different cell lines (Fig. 1C). It is important to note that VEGF is one of many angiogenic molecules (28). As a result, not all tumor types may show strong correlation between tumoral VEGF levels and MVD. However, a positive linear association shows that

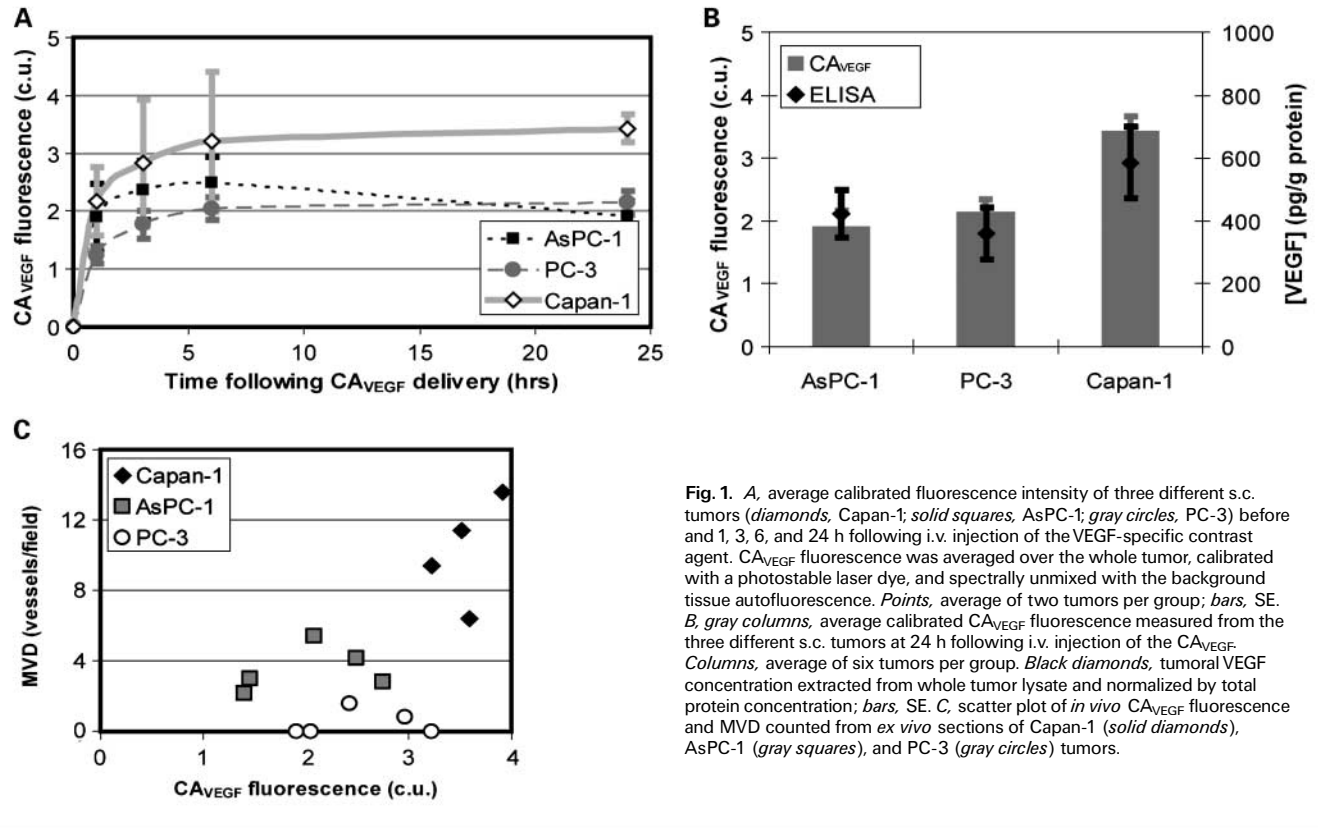

Fig. 1. *A,* average calibrated fluorescence intensity of three different s.c. tumors (*diamonds,* Capan-1; *solid squares,* AsPC-1; *gray circles,* PC-3) before and 1, 3, 6, and 24 h following i.v. injection of the VEGF-specific contrast agent. CA_{VEGF} fluorescence was averaged over the whole tumor, calibrated with a photostable laser dye, and spectrally unmixed with the background tissue autofluorescence. *Points,* average of two tumors per group; *bars,* SE. *B, gray columns,* average calibrated CA_{VEGF} fluorescence measured from the three different s.c. tumors at 24 h following i.v. injection of the CA_{VEGF}. *Columns,* average of six tumors per group. *Black diamonds,* tumoral VEGF concentration extracted from whole tumor lysate and normalized by total protein concentration; *bars,* SE. *C,* scatter plot of *in vivo* CA_{VEGF} fluorescence and MVD counted from *ex vivo* sections of Capan-1 (*solid diamonds*), AsPC-1 (*gray squares*), and PC-3 (*gray circles*) tumors.

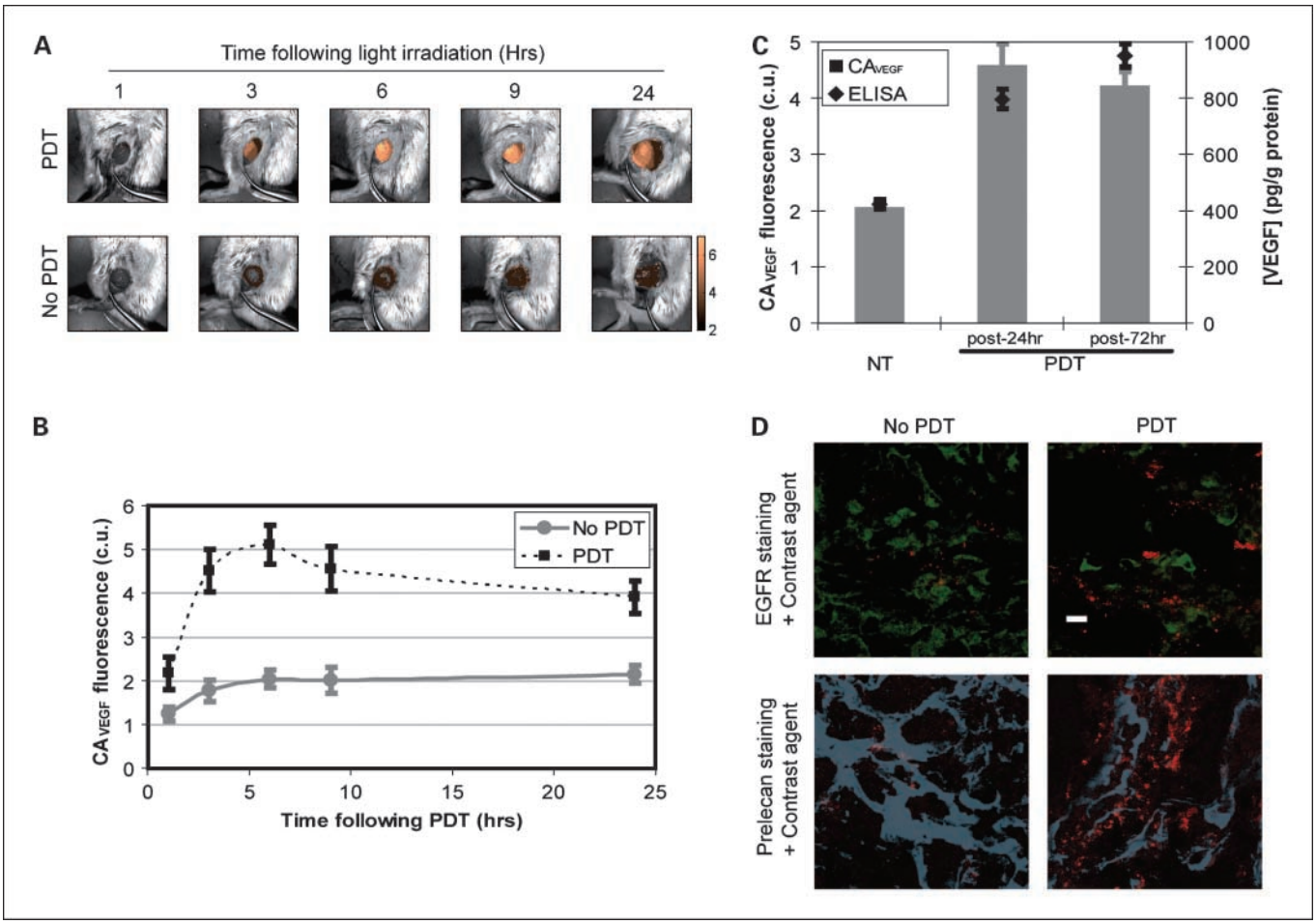

Fig. 2. *A,* labeling of CA_{VEGF} in PDT-treated and nontreated s.c. PC-3 tumors at 1, 3, 6, 9, and 24 h following laser irradiation. The calibrated fluorescence images of tumoral CA_{VEGF} labeling are pseudocolored in gold and overlaid on monochromatic reflectance images. *B,* average calibrated fluorescence intensity of PDT-treated and nontreated PC-3 s.c. tumors 1, 3, 6, 9, and 24 h following laser irradiation. CA_{VEGF} fluorescence was averaged over the whole tumor, calibrated with a photostable laser dye, and spectrally unmixed with the background tissue autofluorescence. *, $P < 0.05$, statistically significant difference between nontreated and PDT-treated groups at each time point. *Points,* average of four tumors per group; *bars,* SE. *C, gray columns,* average calibrated fluorescence intensity of nontreated PC-3 s.c. tumors ($n = 10$) and PDT-treated tumors at 24 h ($n = 16$) and 72 h ($n = 5$) following treatment. *Black diamonds,* corresponding tumoral VEGF concentration extracted from whole tumor lysate and normalized by total protein concentration; *bars,* SE. *D,* immunofluorescence images of cryosections from PDT-treated and nontreated PC-3 s.c. tumors stained for EGFR (*green*) or perlecan (*blue*). The tumored mice were injected i.v. with CA_{VEGF} and treated with PDT. Twenty-four hours following PDT, the tumors were harvested, embedded in OCT compound, and sectioned into 5-μm-thick cryosections. *Red,* localization of the CA_{VEGF}. Bar, 10 μm.

tumoral VEGF measured with CA_{VEGF} plays an important role in angiogenesis (29). Vasculature was not observed in some of the s.c. PC-3 tumors partly because the vasculature in these tumors may not have fully developed at 2 weeks following implantation (data not shown) as well as due to random sampling of the image field within a section of the tumor.

Monitoring VEGF up-regulation following PDT. To test the feasibility of monitoring treatment response with the molecular imaging strategy, CA_{VEGF} labeling was imaged in nontreated and PDT-treated s.c. PC-3 tumors. Figure 2A shows the typical images of CA_{VEGF} labeling in a PDT-treated tumor and a nontreated tumor at different time points following laser irradiation. Statistically significant increase in CA_{VEGF} labeling was observed in PDT-treated tumors as early as 1 hour post-PDT and continued up to 24 hours post-PDT (Fig. 2B).

To validate that the increase in CA_{VEGF} labeling corresponds to post-PDT changes in VEGF expression, tumoral VEGF concentration was quantified *ex vivo* with ELISA from PDT-treated tumors harvested at 24 and 72 hours following treatment. At both time points, PDT-treated tumors showed a 2-fold increase in both tumoral VEGF concentration and CA_{VEGF} labeling, suggesting that the molecular imaging strategy can be used to monitor relative changes in VEGF expression following PDT (Fig. 2C).

To further understand the capabilities of the molecular imaging strategy, spatial localization of the CA_{VEGF} was studied using frozen sections from PDT-treated and nontreated s.c. PC-3 tumors. The sections were stained for human EGFR to visualize the tumor cells (Fig. 2D). Similar to *in vivo* imaging, increased CA_{VEGF} labeling was observed in sections from PDT-treated tumors compared with nontreated tumors. More importantly, CA_{VEGF} labeling did not colocalize with EGFR staining, suggesting that the CA_{VEGF} localizes in the extracellular space and binds to the secreted form of VEGF. VEGF are known to bind to heparan sulfate proteoglycans on cell surface as well as in the basement membrane (30). To investigate the role of proteoglycans, we stained the frozen tumor sections for perlecan, one of the most abundant forms of proteoglycan in

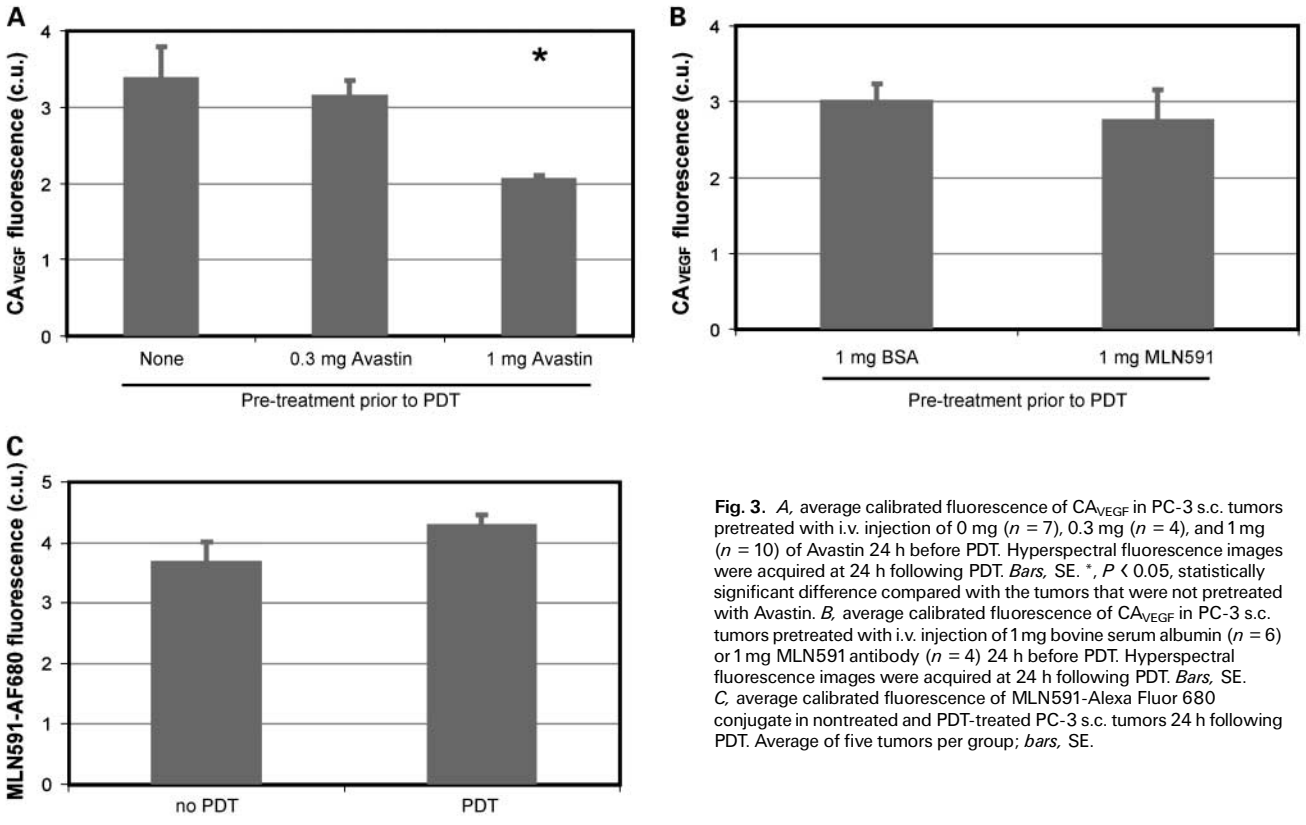

Fig. 3. *A,* average calibrated fluorescence of CA_{VEGF} in PC-3 s.c. tumors pretreated with i.v. injection of 0 mg ($n = 7$), 0.3 mg ($n = 4$), and 1 mg ($n = 10$) of Avastin 24 h before PDT. Hyperspectral fluorescence images were acquired at 24 h following PDT. *Bars,* SE. *, $P < 0.05$, statistically significant difference compared with the tumors that were not pretreated with Avastin. *B,* average calibrated fluorescence of CA_{VEGF} in PC-3 s.c. tumors pretreated with i.v. injection of 1 mg bovine serum albumin ($n = 6$) or 1 mg MLN591 antibody ($n = 4$) 24 h before PDT. Hyperspectral fluorescence images were acquired at 24 h following PDT. *Bars,* SE. *C,* average calibrated fluorescence of MLN591-Alexa Fluor 680 conjugate in nontreated and PDT-treated PC-3 s.c. tumors 24 h following PDT. Average of five tumors per group; *bars,* SE.

tissue (Fig. 2D). In nontreated tumor sections, partial colocalization of the perlecan staining with the CA_{VEGF} is observed, suggesting that the contrast agent labels proteoglycan-bound VEGF as well as those that are unbound. It is interesting to note that colocalization of the perlecan staining with the CA_{VEGF} is not observed in PDT-treated tumor sections, suggesting that most of the VEGF proteins have been released from the extracellular matrix in response to PDT.

Specificity of CA_{VEGF} against VEGF. To investigate CA_{VEGF} specificity against VEGF *in vivo*, we did an *in vivo* antigen blocking experiment. Tumored mice were pretreated with i.v. injection of either 300 μg or 1 mg Avastin 24 hours before PDT. As shown in Fig. 3A, the pretreatment resulted in a decrease in CA_{VEGF} labeling proportional to the dose of Avastin. To further validate that Avastin pretreatment specifically blocks the VEGF protein, tumored mice were pretreated 24 hours before PDT with i.v. injection of either 1 mg bovine serum albumin or 1 mg MLN591 anti-prostate-specific membrane antigen antibody that do not bind to VEGF and should not affect CA_{VEGF} labeling. Pretreatment with bovine serum albumin and with MLN591 did not result in a statistically significant change in CA_{VEGF} labeling (Fig. 3B).

PDT is known to induce physiologic changes in vascular permeability (31), which could increase tumoral CA_{VEGF} uptake regardless of the changes in tumoral VEGF concentration. The effect of PDT-induced vascular permeability on labeling of antibody-based contrast agents was investigated using MLN591, as prostate-specific membrane antigen expression does not change with PDT in s.c. PC-3 tumors (data not shown). *In vivo* labeling of MLN591 conjugated with Alexa Fluor 680 did not show significant difference between PDT-treated and nontreated tumors (Fig. 3C), suggesting that the PDT treatment did not result in nonspecific uptake of the fluorescently labeled antibody.

Targeting efficiency of CA_{VEGF}. Although Fig. 3 shows specificity of CA_{VEGF} against VEGF, it is not clear how much tumoral VEGF is labeled by CA_{VEGF}. To study the targeting efficiency, average CA_{VEGF} fluorescence intensity in Fig. 1A was converted to total tumoral CA_{VEGF} concentration using a standard curve generated with pulverized tumors (Supplementary Fig. S1). Then, $[CA_{VEGF}]_{Bound}$ and $[CA_{VEGF}]_{Free}$ were determined by fitting the mathematical model to the total tumoral CA_{VEGF} concentration determined from the fluorescence images (Supplementary Fig. S2). Table 1 shows the values of PS and L estimated by the model-based quantitative analysis and the resulting $[CA_{VEGF}]_{Bound}$ and $[CA_{VEGF}]_{Free}$. The estimates of PS and L were comparable with values determined in tumors (22, 32). The ratio of $[CA_{VEGF}]_{Bound}$ and $[CA_{VEGF}]_{Free}$ shows approximately 80% of CA_{VEGF} delivered to the tumor are bound to VEGF in all three tumors, confirming CA_{VEGF} specificity. However, CA_{VEGF} delivered to the tumor labels only about 40% to 60% of the total tumoral VEGF determined by ELISA (Fig. 4).

Discussion

VEGF plays a pivotal role in tumor angiogenesis, tumor growth, and metastasis and has been widely reported as a

Table 1. Variables input to and estimated by fitting the pharmacokinetic model to the CA_{VEGF} labeling in PC-3, AsPC-1, and Capan-1 tumors

	[VEGF] (nmol/L)*	$[CA_{VEGF}]_{Bound}$ (nmol/L) †	$[CA_{VEGF}]_{Free}$ (nmol/L) †	PS (mL/min/g) †,‡	*L* (mL/min/g) †,‡
PC-3	10.1 ± 0.2	5.1 ± 0.07	1.1 ± 0.03	0.08 ± 0.005	6.4 ± 0.3
AsPC-1	11.7 ± 0.2	5.8 ± 0.1	1.1 ± 0.05	0.12 ± 0.006	10.0 ± 0.0
Capan-1	15.6 ± 0.3	8.6 ± 0.1	1.3 ± 0.04	0.14 ± 0.01	9.6 ± 0.3

*Variable that was determined *ex vivo* by ELISA and input to the pharmacokinetic model.
† Margin of error was derived from a potential 15 % variation in CA_{VEGF} circulation half life.
‡ Variables estimated by the pharmacokinetic model.

significant prognostic indicator of patient survival (33–36). At the same time, there are reports that VEGF does not provide significant prognostic information (4, 6, 37). In fact, the xenograft models of human pancreatic cancer show higher level of VEGF with the AsPC-1 cell line compared with Capan-1 (Fig. 1), but it is the Capan-1 that develops into a more aggressive phenotype (38, 39). The understanding of the complexity of the role VEGF plays in tumor development has been somewhat limited by the absence of methods of *in situ* measurement of this cytokine spatially and temporally. Although the snapshot of VEGF levels measured in circulation or *ex vivo* may reflect overall VEGF levels, subtle differences in its spatial distribution and temporal change can have a major effect on prognosis and treatment response. For example, localized microenvironmental VEGF concentration and the spatial redistribution of VEGF in different tissue compartments have been shown to play an important role in aberrant angiogenesis and cancer progression (18, 19, 40). As a result, capabilities to monitor the spatial and temporal dynamics of VEGF expression *in vivo* can provide more robust and accurate information regarding disease progression and appropriate targeted intervention strategies.

Here, we developed an optical molecular imaging strategy to monitor VEGF expression and its dynamics in various tumors and following cancer therapy. Average CA_{VEGF} labeling in three different tumors (Fig. 1) as well as following PDT (Fig. 2) correlated well with the tumoral VEGF concentration determined *ex vivo*. Furthermore, a more quantitative analysis using a pharmacokinetic model shows that *in vivo* CA_{VEGF} labeling is proportional to and labels approximately half of the tumoral VEGF concentration (Fig. 4), demonstrating that the VEGF imaging strategy can be used to monitor the tumoral VEGF levels. The fact that *in vivo* CA_{VEGF} labeling is associated with the MVD further shows that VEGF detected by the imaging strategy is functionally active in promoting angiogenesis (Fig. 1C).

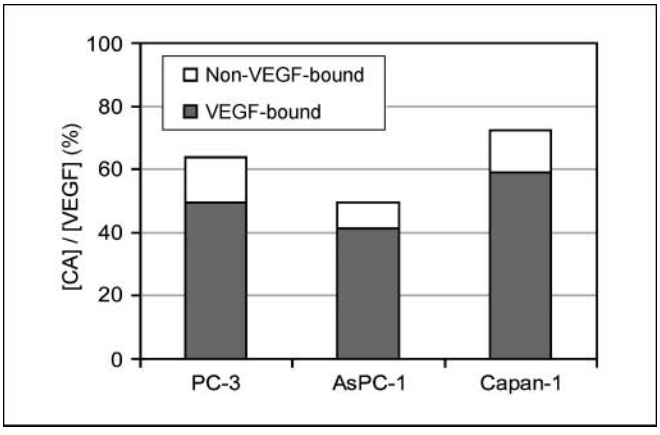

Fig. 4. Targeting efficiency of the VEGF-specific contrast agent in three different tumors (PC-3, AsPC-1, and Capan-1). Targeting efficiency is calculated as the ratio of the tumoral CA_{VEGF} concentration determined from the hyperspectral images to the tumoral VEGF concentration determined by ELISA. The concentration of the VEGF-bound and unbound CA_{VEGF} concentrations were estimated using pharmacokinetic model-based quantitative analysis.

Because of its complexity, the *in vivo* environment can lead to nonspecific binding of molecular specific contrast agents. In particular, *in vivo* specificity of contrast agents targeted at nonanchored cytokines has not been studied previously. We rigorously tested the specificity of CA_{VEGF} using various approaches. *In vivo* antigen blocking experiment shows that Avastin pretreatment before imaging blocks the tumoral VEGF and that CA_{VEGF} labeling decreased in proportion to the pretreated Avastin dose, showing that CA_{VEGF} specifically binds to the VEGF protein *in vivo* (Fig. 3). In fact, quantitative analysis using the pharmacokinetic model shows approximately 80% of the CA_{VEGF} delivered to the tumor is bound to VEGF (Fig. 4). In addition to the specificity of the contrast agent to its antigen, any physiologic changes could also affect the specificity of the contrast agent labeling. Investigation with a fluorescently labeled antibody against prostate-specific membrane antigen, whose levels do not change with PDT, showed that PDT conditions used in this study do not affect the delivery of antibody-based contrast agents to the tumor (Fig. 3). However, it is still possible that vascular targeting PDT resulting in a significant change in vascular permeability (31) could potentially increase nonspecific uptake of antibody-based contrast agents as observed in ref. 41.

In addition to analyzing the overall CA_{VEGF} labeling in tumors, microscopic localization of CA_{VEGF} was investigated using immunohistochemistry of tumors labeled with CA_{VEGF} *in vivo* (Fig. 2D). CA_{VEGF} did not colocalize with EGFR staining, suggesting that the contrast agent labels the VEGF proteins localized in the extracellular space. More importantly, potential release of VEGF from extracellular matrix following PDT was observed from sections stained for proteoglycans. Although the precise mechanism needs further investigation, PDT-generated reactive oxygen could potentially degrade proteoglycans and release heparin-binding growth factors (42). Along with cell-secreted VEGF (9), heparin-binding VEGF released from the extracellular matrix by PDT may also play an important role in tumor growth and metastasis (43). These microscopic temporal

and spatial details can potentially be probed *in vivo* and in a minimally invasive manner by combining the VEGF imaging strategy with high-resolution fluorescence endoscopic imaging system (44).

Capabilities to monitor VEGF expression following cancer treatment is particularly important as cancer treatments including radiotherapy (7), chemotherapy (8), and PDT (9) can lead to increased expression of VEGF and potentially stimulate tumor regrowth and metastasis to distant organs (10, 11). Combination with antiangiogenic therapies enhanced the antitumor effect and reduced the metastatic burden of these treatments (45, 46), strongly suggesting that post-treatment VEGF expression plays an important role in recurrent disease and metastasis. Capabilities of the *in vivo* optical molecular imaging strategy to monitor changes in tumoral VEGF expression following PDT can potentially be used to monitor the response in these different treatment modalities.

In addition to contrast agent specificity, decrease in CA_{VEGF} labeling following Avastin pretreatment (Fig. 3A) also show the capabilities to monitor the pharmacodynamics of Avastin, an antiangiogenic agent. *In situ, in vivo* monitoring of anti-angiogenic agent pharmacodynamics can potentially help optimize treatment planning for these novel therapies (47). As a result, the *in vivo* VEGF imaging strategy reported here can potentially help predict the treatment response, monitor the pharmacodynamics of antiangiogenic agents, and plan appropriate intervention strategies.

As shown in Fig. 4, the concentration of $[CA_{VEGF}]_{Total}$ is approximately 50% of the tumoral VEGF concentration, suggesting that CA_{VEGF} labels approximately half the VEGF protein in the tumor. The relatively low targeting efficiency could be partly explained by the fact that the *ex vivo* ELISA assay measures both the intracellular and the extracellular VEGF, whereas the contrast agent targets only the extracellular protein. Another possible explanation is the limited penetration of antibodies in solid tumors (48), compromising the delivery of antibody-based CA_{VEGF} in tumor regions distant from blood vessels. The targeting efficiency of the CA_{VEGF} can potentially be improved by using targeting agents other than antibodies with enhanced tumor penetration.

Optical imaging, particularly planar macroscopic imaging used in this report, is inherently limited by the depth of light penetration in tissue ($\sim$2 mm; ref. 49). However, recent advances in optical imaging technologies such as endoscopy (44) can help access to organs deep inside the body. Tumors that are large in size can still pose a challenge due to limited field of view and depth of imaging associated with optical technologies. Advances in optical imaging technologies such as diffuse optical tomography will potentially enable interrogation of whole organs (50). At the same time, the molecular imaging strategy investigated in this report can be applied to other imaging modalities with whole-body imaging capabilities such as nuclear imaging if interrogation of a large volume is necessary. The molecular imaging strategy described in this report in combination with these technologies can help monitor VEGF expression *in vivo* in various organ sites.

In summary, we report an optical molecular imaging strategy to monitor VEGF expression *in vivo*. Experimental results show that the antibody-based CA_{VEGF} labeled VEGF proteins with high specificity. The molecular imaging strategy was capable of monitoring VEGF levels in different tumors as well as changes in VEGF expression following a therapeutic intervention such as PDT and Avastin treatment. These capabilities could potentially serve as a useful tool for monitoring treatment response, studying mechanisms, and designing appropriate mechanism-based interventions in the future.

Disclosure of Potential Conflicts of Interest

No potential conflicts of interest were disclosed.

Acknowledgments

We thank Genentech for Avastin, Millennium Pharmaceuticals for MLN591, ImClone Systems for C225, and QLT for benzoporphyrin derivative.

References

1. Dvorak HF. Vascular permeability factor/vascular endothelial growth factor: a critical cytokine in tumor angiogenesis and a potential target for diagnosis and therapy. J Clin Oncol 2002;20:4368–80.
2. Kuwahara K, Sasaki T, Kuwada Y, Murakami M, Yamasaki S, Chayama K. Expressions of angiogenic factors in pancreatic ductal carcinoma: a correlative study with clinicopathologic parameters and patient survival. Pancreas 2003;26:344–9.
3. Bok RA, Halabi S, Fei DT, et al. Vascular endothelial growth factor and basic fibroblast growth factor urine levels as predictors of outcome in hormone-refractory prostate cancer patients: a cancer and leukemia group B study. Cancer Res 2001;61:2533–6.
4. Borre M, Nerstrom B, Overgaard J. Association between immunohistochemical expression of vascular endothelial growth factor (VEGF), VEGF-expressing neuroendocrine-differentiated tumor cells, and outcome in prostate cancer patients subjected to watchful waiting. Clin Cancer Res 2000; 6:1882–90.
5. Galizia G, Lieto E, Ferraraccio F, et al. Determination of molecular marker expression can predict clinical outcome in colon carcinomas. Clin Cancer Res 2004; 10:3490–9.
6. Khorana AA, Ryan CK, Cox C, Eberly S, Sahasrabudhe DM. Vascular endothelial growth factor, CD68, and epidermal growth factor receptor expression and survival in patients with stage II, stage III colon carcinoma: a role for the host response in prognosis. Cancer 2003;97:960–8.
7. Gorski DH, Beckett MA, Jaskowiak NT, et al. Blockage of the vascular endothelial growth factor stress response increases the antitumor effects of ionizing radiation. Cancer Res 1999;59:3374–8.
8. Viloria-Petit A, Crombet T, Jothy S, et al. Acquired resistance to the antitumor effect of epidermal growth factor receptor-blocking antibodies *in vivo*: a role for altered tumor angiogenesis. Cancer Res 2001;61: 5090–101.
9. Solban N, Selbo PK, Sinha AK, Chang SK, Hasan T. Mechanistic investigation and implications of PDT-induction of VEGF in prostate cancer. Cancer Res 2006;66:1–8.
10. Camphausen K, Moses MA, Beecken WD, Khan MK, Folkman J, O'Reilly MS. Radiation therapy to a primary tumor accelerates metastatic growth in mice. Cancer Res 2001;61:2207–11.
11. Momma T, Hamblin MR, Wu HC, Hasan T. Photodynamic therapy of orthotopic prostate cancer with benzoporphyrin derivative: local control and distant metastasis. Cancer Res 1998;58:5425–31.
12. Vermeulen PB, Gasparini G, Fox SB, et al. Second international consensus on the methodology and criteria of evaluation of angiogenesis quantification in solid human tumours. Eur J Cancer 2002;38: 1564–79.
13. Hasan J, Shnyder SD, Bibby M, Double JA, Bicknel R, Jayson GC. Quantitative angiogenesis assays *in vivo*—a review. Angiogenesis 2004;7:1–16.
14. Henson DE. Back to the drawing board on immunohistochemistry and predictive factors. J Natl Cancer Inst 2005;97:1796–7.
15. Backer MV, Levashova Z, Patel V, et al. Molecular imaging of VEGF receptors in angiogenic vasculature with single-chain VEGF-based probes. Nat Med 2007;13:504–9.
16. Bremer C, Bredow S, Mahmood U, Weissleder R, Tung CH. Optical imaging of matrix metalloproteinase-2 activity in tumors: feasibility study in a mouse model. Radiology 2001;221:523–9.
17. Kumar R, Kuniyasu H, Bucana CD, Wilson MR, Fidler IJ. Spatial and temporal expression of angiogenic molecules during tumor growth and progression. Oncol Res 1998;10:301–11.
18. Huss WJ, Hanrahan CF, Barrios RJ, Simons JW, Greenberg NM. Angiogenesis and prostate cancer: identification of a molecular progression switch. Cancer Res 2001;61:2736–43.
19. Itakura J, Ishiwata T, Friess H, et al. Enhanced expression of vascular endothelial growth factor in

human pancreatic cancer correlates with local disease progression. Clin Cancer Res 1997;3:1309–16.

20. Jayson GC, Zweit J, Jackson A, et al. Molecular imaging and biological evaluation of HuMV833 anti-VEGF antibody: implications for trial design of antiangiogenic antibodies. J Natl Cancer Inst 2002; 94:1484–93.

21. Drexhage KH. Structure and properties of laser dyes. In: Schaefer FP, editor. Dye lasers. 1st ed. Heidelberg: Springer Berlin; 1973. p. 155–200.

22. Sung C, Shockley TR, Morrison PF, Dvorak HF, Yarmush ML, Dedrick RL. Predicted and observed effects of antibody affinity and antigen density on monoclonal antibody uptake in solid tumors. Cancer Res 1992;52:377–84.

23. Gerber HP, Ferrara N. Pharmacology and pharmacodynamics of bevacizumab as monotherapy or in combination with cytotoxic therapy in preclinical studies. Cancer Res 2005;65:671–80.

24. Savellano MD, Hasan T. Photochemical targeting of epidermal growth factor receptor: a mechanistic study. Clin Cancer Res 2005;11:1658–68.

25. Folli S. Antibody-indocyanin conjugates for immunophotodetection of human squamous cell carcinoma in nude mice. Cancer Res 1994;54:2643–9.

26. Pelegrin A, Folli S, Buchegger F, Mach JP, Wagnieres G, van den Bergh H. Antibody-fluorescein conjugates for photoimmunodiagnosis of human colon carcinoma in nude mice. Cancer 1991;67: 2529–37.

27. Lin YS, Nguyen C, Mendoza JL, et al. Preclinical pharmacokinetics, interspecies scaling, and tissue distribution of a humanized monoclonal antibody against vascular endothelial growth factor. J Pharmacol Exp Ther 1999;288:371–8.

28. Carmeliet P, Jain RK. Angiogenesis in cancer and other diseases. Nature 2000;407:249–57.

29. Hicklin DJ, Ellis LM. Role of the vascular endothelial growth factor pathway in tumor growth and angiogenesis. J Clin Oncol 2005;23:1011–27.

30. Jiang X, Couchman JR. Perlecan and tumor angiogenesis. J Histochem Cytochem 2003;51:1393–410.

31. Chen B, Pogue BW, Luna JM, Hardman RL, Hoopes PJ, Hasan T. Tumor vascular permeabilization by vascular-targeting photosensitization: effects, mechanism, and therapeutic implications. Clin Cancer Res 2006; 12:917–23.

32. Butler TP, Grantham FH, Gullino PM. Bulk transfer of fluid in the interstitial compartment of mammary tumors. Cancer Res 1975;35:3084–8.

33. Gasparini G. Prognostic value of vascular endothelial growth factor in breast cancer. Oncologist 2000;5 Suppl 1:37–44.

34. Garcea G, Neal CP, Pattenden CJ, Steward WP, Berry DP. Molecular prognostic markers in pancreatic cancer: a systematic review. Eur J Cancer 2005;41: 2213–36.

35. Delongchamps NB, Peyromaure M, Dinh-Xuan AT. Role of vascular endothelial growth factor in prostate cancer. Urology 2006;68:244–8.

36. Des Guetz G, Uzzan B, Nicolas P, et al. Microvessel density and VEGF expression are prognostic factors in colorectal cancer. meta-analysis of the literature. Br J Cancer 2006;94:1823–32.

37. Fujimoto K, Hosotani R, Wada M, et al. Expression of two angiogenic factors, vascular endothelial growth factor and platelet-derived endothelial cell growth factor in human pancreatic cancer, and its relationship to angiogenesis. Eur J Cancer 1998;34: 1439–47.

38. Hotz HG, Reber HA, Hotz B, et al. An orthotopic nude mouse model for evaluating pathophysiology and therapy of pancreatic cancer. Pancreas 2003;26: e89–98.

39. Loukopoulos P, Kanetaka K, Takamura M, Shibata T, Sakamoto M, Hirohashi S. Orthotopic transplantation models of pancreatic adenocarcinoma derived from cell lines and primary tumors and displaying varying metastatic activity. Pancreas 2004;29:193–203.

40. Ozawa CR, Banfi A, Glazer NL, et al. Microenvironmental VEGF concentration, not total dose, determines a threshold between normal and aberrant angiogenesis. J Clin Invest 2004;113:516–27.

41. Hu P, Hornick JL, Glasky MS, et al. A chimeric Iym-1/interleukin 2 fusion protein for increasing tumor vascular permeability and enhancing antibody uptake. Cancer Res 1996;56:4998–5004.

42. Metcalfe DD, Thompson HL, Klebanoff SJ, Henderson WR, Jr. Oxidative degradation of rat mast-cell heparin proteoglycan. Biochem J 1990;272:51–7.

43. Vlodavsky I, Friedmann Y. Molecular properties and involvement of heparanase in cancer metastasis and angiogenesis. J Clin Invest 2001;108:341–7.

44. Jung JC, Mehta AD, Aksay E, Stepnoski R, Schnitzer MJ. *In vivo* mammalian brain imaging using one- and two-photon fluorescence microendoscopy. J Neurophysiol 2004;92:3121–33.

45. Gorski DH, Mauceri HJ, Salloum RM, Halpern A, Seetharam S, Weichselbaum RR. Prolonged treatment with angiostatin reduces metastatic burden during radiation therapy. Cancer Res 2003;63: 308–11.

46. Kosharskyy B, Solban N, Chang SK, Rizvi I, Chang Y, Hasan T. A mechanism-based combination therapy reduces local tumor growth and metastasis in an orthotopic model of prostate cancer. Cancer Res 2006;66:10953–8.

47. Emmenegger U, Kerbel RS. A dynamic de-escalating dosing strategy to determine the optimal biological dose for antiangiogenic drugs. Clin Cancer Res 2005; 11:7589–92.

48. Jain M, Venkatraman G, Batra SK. Optimization of radioimmunotherapy of solid tumors: biological impediments and their modulation. Clin Cancer Res 2007;13:1374–82.

49. Weissleder R, Mahmood U. Molecular imaging. Radiology 2001;219:316–33.

50. Gibson AP, Hebden JC, Arridge SR. Recent advances in diffuse optical imaging. Phys Med Biol 2005; 50:R1–43.